

Modal method for the 2D wave propagation in heterogeneous anisotropic media

AGNÈS MAUREL,^{1,*} JEAN-FRANÇOIS MERCIER,² AND SIMON FÉLIX³

¹Institut Langevin, CNRS, ESPCI ParisTech, 1 rue Jussieu, 75005 Paris, France

²Poems, CNRS, ENSTA ParisTech, INRIA, 828 boulevard des Maréchaux, 91762 Palaiseau, France

³LAUM, CNRS, Université du Maine, avenue Olivier Messiaen, 72085 Le Mans, France

*Corresponding author: agnes.maurel@espci.fr

Received 10 December 2014; revised 23 March 2015; accepted 23 March 2015; posted 24 March 2015 (Doc. ID 229012); published 30 April 2015

A multimodal method based on a generalization of the admittance matrix is used to analyze wave propagation in heterogeneous two-dimensional anisotropic media. The heterogeneity of the medium can be due to the presence of anisotropic inclusions with arbitrary shapes, to a succession of anisotropic media with complex interfaces between them, or both. Using a modal expansion of the wave field, the problem is reduced to a system of two sets of first-order differential equations for the modal components of the field, similar to the system obtained in the rigorous coupled wave analysis. The system is solved numerically, using the admittance matrix, which leads to a stable numerical method, the basic properties of which are discussed. The convergence of the method is discussed, considering arrays of anisotropic inclusions with complex shapes, which tend to show that Li's rules are not concerned within our approach. The method is validated by comparison with a subwavelength layered structure presenting an effective anisotropy at the wave scale. © 2015 Optical Society of America

OCIS codes: (260.2110) Electromagnetic optics; (050.1950) Diffraction gratings; (160.1190) Anisotropic optical materials; (160.3918) Metamaterials.

<http://dx.doi.org/10.1364/JOSAA.32.000979>

1. INTRODUCTION

The propagation of electromagnetic waves in anisotropic media is a topic that has been addressed for many years, originally because such materials can be found in nature: crystals and liquid crystals provide important different classes of optically anisotropic media, and they are commonly used in optical devices as light modulators [1], polarizers [2], narrowband filters [3], and optical fibers [4]. More recently, interest in such complex media has been renewed because man-made materials present an artificial, or effective, anisotropy, which can be engineered by assigning the value of each parameter of the permeability and/or permittivity tensors to be positive, near zero, or even negative [5]. It results in a larger flexibility to manipulate the wave propagation. These anisotropic materials have been extensively investigated to achieve new wave phenomena in the field of imaging below the diffraction limit [6,7], subdiffraction guidance [8,9], including dissipative effects [10] and nonlinear effects [11], microstructures optical fiber [12], or sensing [13].

Due to the complexity of anisotropy, analytical solutions are usually not available and numerical modeling is needed (for reviews on the numerical methods, see, e.g., [14,15]). Among the different numerical approaches, modal methods are, in general,

well adapted to describe the propagation in waveguides and in periodic systems. This is because the dependence of the solution on one or two of the spatial coordinates can be encapsulated in a set of functions forming a basis, thus reducing the problem to one (or two) dimensions.

Many studies have focused on the case of stratified (or multilayered) anisotropic media with plane interfaces [16–20]; obviously, this problem can be solved analytically, but, when many layers are considered, the obtained expressions of the solution become intractable. Starting in 2001, the Fourier method (or rigorous coupled wave analysis) has been adapted to describe wave scattering by anisotropic gratings with complex interface [21–24]. The Fourier method relies on a formulation of the harmonic Maxwell's equations in Fourier space for periodic structures, resulting in a first-order system of differential equations, with special attention being paid on Li's, or Laurent's, factorization rules [25]. We also mention the paper from Li [26], which uses a coordinate transformation (Chandezon method) for periodically modulated anisotropic layers with a shape edge interface.

The present study follows from a previous one where a multimodal method, similar to the Fourier method, was used to analyze wave propagation through isotropic scatterers of

arbitrary shapes, located in a waveguide or periodically located on an array [27]. We extend this modal method to anisotropic media, with a restriction to uniaxial media, or biaxial media being orientated such that no cross polarization occurs in the incident plane (for either TE or TM); thus, the problem remains two dimensional.

The paper is organized as follows. In Section 2, the derivation of the set of first-order differential equations is presented. In the TM case, it involves the modal components of the magnetic field H and of a related quantity, denoted E , which appears naturally from the weak formulation of the problem. Section 3 presents the numerical resolution of the system; it is based on the use of a generalized impedance matrix, similar to the electromagnetic impedance, which links, locally, the modal components of E and H . The impedance matrix satisfies a Riccati equation, which can be properly integrated, starting from the radiation condition. In Section 4, results on the convergence and validations are presented; through the example of arrays of inclusions with different shapes, we inspect the convergence of the method, notably with respect to the staircase approximation [28]. Next, a validation of the method is proposed, by comparison with reference calculations of the scattering by subwavelength layered media, which are known to behave as equivalent anisotropic media.

We report in the appendices some technical calculations, which concern notably the numerical integration of the impedance matrix, using a Magnus scheme.

2. DERIVATION OF THE MULTIMODAL FORMULATION

The propagation of electromagnetic waves in anisotropic heterogeneous media is described by the Maxwell's equations, with electric and magnetic permittivity being tensors. In the harmonic regime, and assuming time dependance $e^{-i\omega t}$, we have $\nabla \cdot \mathbf{D} = 0$, $\nabla \cdot \mathbf{B} = 0$, $\nabla \times \mathbf{E} = ik\mathbf{B}$, and $\nabla \times \mathbf{H} = -ik\mathbf{D}$, where $k \equiv \omega/c$ denotes the wavenumber in free space, c being the celerity in the free space (as free space does not compose necessarily one of the media, basically, k is used to denote the frequency). We restrict our study to anisotropic media with no spatial dispersion; thus, the permittivity tensor (or dielectric tensor) $\boldsymbol{\varepsilon}$ is symmetric [29] with $\boldsymbol{\varepsilon} = \text{diag}(\varepsilon_X, \varepsilon_Y, \varepsilon_Z)$ when expressed in the frame (X, Y, Z) of the principal directions of anisotropy. The media have scalar permeabilities μ . In this section, we establish the multimodal formulation [Eq. (15)]. The derivation is performed using a weak formulation of the problem and expanding the solution onto a basis of transverse functions $\varphi_n(x)$. The multimodal formulation is presented in the case of periodic media (Fig. 1) for TM waves, the case of TE waves being reduced to isotropic media.

A. Notations

We denote (x, y, z) the reference frame associated to the periodic structure, and we consider anisotropic media with the principal axes of anisotropy X and Y being rotated along the $Z = z$ direction through an angle α . In the reference frame,

$$\mathbf{D} = {}^t\mathbf{R}_\alpha^{(3D)} \begin{pmatrix} \varepsilon_X & 0 & 0 \\ 0 & \varepsilon_Y & 0 \\ 0 & 0 & \varepsilon_Z \end{pmatrix} \mathbf{R}_\alpha^{(3D)} \mathbf{E}, \quad \text{with} \quad \mathbf{R}_\alpha^{(3D)} \equiv \begin{pmatrix} \cos \alpha & \sin \alpha & 0 \\ -\sin \alpha & \cos \alpha & 0 \\ 0 & 0 & 1 \end{pmatrix}. \quad (1)$$

In TM polarization, we obtain $\mathbf{H} = H(x, y)\mathbf{e}_z$ and $\mathbf{E} = E_x(x, y)\mathbf{e}_x + E_y(x, y)\mathbf{e}_y$, leading to

$$\nabla \cdot \left[{}^t\mathbf{R}_\alpha \begin{pmatrix} \varepsilon_Y^{-1} & 0 \\ 0 & \varepsilon_X^{-1} \end{pmatrix} \mathbf{R}_\alpha \nabla H \right] + k^2 \mu H = 0, \quad \text{with} \quad \mathbf{R}_\alpha \equiv \begin{pmatrix} \cos \alpha & \sin \alpha \\ -\sin \alpha & \cos \alpha \end{pmatrix}, \quad (2)$$

and all the parameters α , ε_X , ε_Y , and μ vary in space. Evidently, the result applies for uniaxial media and $\varepsilon_Z = \varepsilon_X$ or $\varepsilon_Z = \varepsilon_Y$, in which case any rotation in the 3D space can be considered. In the following, we use the notations

$$\begin{cases} \nabla \cdot \left[\begin{pmatrix} \varepsilon_{xx}^{-1} & \varepsilon_{xy}^{-1} \\ \varepsilon_{xy}^{-1} & \varepsilon_{yy}^{-1} \end{pmatrix} \nabla H \right] + k^2 \mu H = 0, \\ -ikE_x = \varepsilon_{xy}^{-1} \partial_x H + \varepsilon_{yy}^{-1} \partial_y H, \quad ikE_y = \varepsilon_{xx}^{-1} \partial_x H + \varepsilon_{xy}^{-1} \partial_y H, \end{cases} \quad (3)$$

$$\begin{aligned} \text{with} \quad \varepsilon_{xx}^{-1} &\equiv \varepsilon_Y^{-1} \cos^2 \alpha + \varepsilon_X^{-1} \sin^2 \alpha, \\ \varepsilon_{xy}^{-1} &\equiv (\varepsilon_Y^{-1} - \varepsilon_X^{-1}) \cos \alpha \sin \alpha, \\ \varepsilon_{yy}^{-1} &\equiv \varepsilon_Y^{-1} \sin^2 \alpha + \varepsilon_X^{-1} \cos^2 \alpha. \end{aligned} \quad (4)$$

Our notations for the inverse permittivities ε_{ij}^{-1} in Eqs. (4) are not usual, but they are more tractable for the following. We report in Appendix A the link with the permittivity tensor $\boldsymbol{\varepsilon}$, as defined in the relation $\mathbf{D} = \boldsymbol{\varepsilon}\mathbf{E}$.

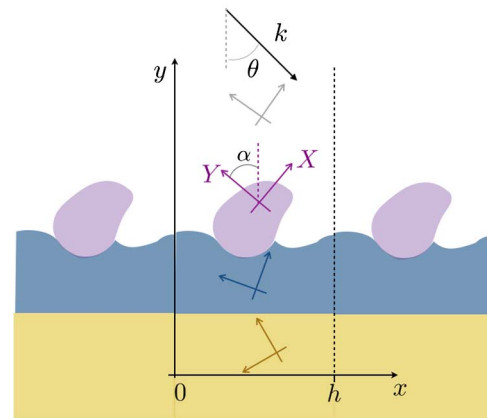


Fig. 1. Typical configuration of the study. An incident wave with wave vector \mathbf{k} at incidence θ propagates through a succession of layers and inclusions being h periodic along the x direction. Each layer or inclusion may be composed of an anisotropic medium with principal directions (X, Y) tilted through an angle α with respect to the (x, y) frame associated to the periodic structure.

B. Multimodal Formulation

We consider a periodic configuration with h periodicity along the x axis (Fig. 1). Following [27], the wave in Eq. (3) is written in a variational representation:

$$\sum_i \int_{\Omega_i} d\mathbf{r} \left[- \begin{pmatrix} \varepsilon_{xx}^{-1} & \varepsilon_{xy}^{-1} \\ \varepsilon_{xy}^{-1} & \varepsilon_{yy}^{-1} \end{pmatrix} \nabla H \cdot \nabla \tilde{H}_t + k^2 \mu H \tilde{H}_t \right] + \sum_i \int_{\partial\Omega_i} dS \begin{pmatrix} \varepsilon_{xx}^{-1} & \varepsilon_{xy}^{-1} \\ \varepsilon_{xy}^{-1} & \varepsilon_{yy}^{-1} \end{pmatrix} \nabla H \cdot \mathbf{n} \tilde{H}_t = 0, \quad (5)$$

where Ω_i denotes the regions with constant $(\varepsilon_{xx}^{-1}, \varepsilon_{xy}^{-1}, \varepsilon_{yy}^{-1})$ and μ values; for readability, we avoid indicating explicitly the index (i) on these values. In the above expression, $H_t(\mathbf{r})$ is a test function compactly supported (thus, vanishing for $y \rightarrow \pm\infty$) and h periodic along x ; its form will be given below. The last integral vanishes because of the boundary conditions at $\partial\Omega_i$, being either the boundary between two different media (continuity of $[\begin{pmatrix} \varepsilon_{xx}^{-1} & \varepsilon_{xy}^{-1} \\ \varepsilon_{xy}^{-1} & \varepsilon_{yy}^{-1} \end{pmatrix} \nabla H] \cdot \mathbf{n}$), or the boundary of the domain $x = 0$ and $x = h$ (and the conditions of periodicity give $[(\varepsilon_{xx}^{-1} \partial_x H + \varepsilon_{xy}^{-1} \partial_y H) \tilde{H}_t](x = h) = [(\varepsilon_{xx}^{-1} \partial_x H + \varepsilon_{xy}^{-1} \partial_y H) \tilde{H}_t](x = 0)$). For $y \rightarrow \pm\infty$, it vanishes because H_t vanishes. Thus, the boundary conditions have been exactly taken into account in the weak formulation:

$$\sum_i \int_{\Omega_i} d\mathbf{r} \left[- \begin{pmatrix} \varepsilon_{xx}^{-1} & \varepsilon_{xy}^{-1} \\ \varepsilon_{xy}^{-1} & \varepsilon_{yy}^{-1} \end{pmatrix} \nabla H \cdot \nabla \tilde{H}_t + k^2 \mu H \tilde{H}_t \right] = 0. \quad (6)$$

We now expand $H(x, y)$ onto a basis of $\varphi_m(x)$ (with Einstein summation convention),

$$H(x, y) = H_m(y) \varphi_m(x), \quad (7)$$

and the φ_m functions are chosen as

$$\varphi_m(x) = \frac{1}{\sqrt{h}} e^{i\gamma_m x}, \quad \text{with } \gamma_m \equiv (\kappa + 2m\pi/h), \quad (8)$$

where $e^{i\kappa x}$ denotes the dependence of the waves in the x direction, imposed by the source term (the incident wave). We now use the following form of the test function: $H_t(\mathbf{r}) = H_t(y) \varphi_n(x)$, with arbitrary n value. Integrating Eq. (6) over x , the equation ends with $\int dy \tilde{H}_t(y) F(y) = 0$ for any H_t , from which $F(y) = 0$ is deduced. This leads to

$$\frac{d}{dy} \left[\sum_i (\varepsilon_{yy}^{-1} \mathbf{A}_{nm} H_m' + \varepsilon_{xy}^{-1} \mathbf{B}_{nm} H_m) \right] + \sum_i (-\varepsilon_{xy}^{-1} \overline{\mathbf{B}}_{nm} H_m' - \varepsilon_{xx}^{-1} \mathbf{C}_{nm} H_m + k^2 \mu \mathbf{A}_{nm} H_m) = 0, \quad (9)$$

where we have defined the matrices:

$$\begin{cases} \mathbf{A}_{nm}(y) \equiv \int_{a_i(y)}^{a_{i+1}(y)} dx \overline{\varphi_n(x)} \varphi_m(x), \\ \mathbf{B}_{nm}(y) \equiv \int_{a_i(y)}^{a_{i+1}(y)} dx \overline{\varphi_n(x)} \varphi_m'(x), \\ \mathbf{C}_{nm}(y) \equiv \int_{a_i(y)}^{a_{i+1}(y)} dx \overline{\varphi_n'(x)} \varphi_m'(x). \end{cases} \quad (10)$$

The $a_i(y)$ is a parametrization of the boundaries of the (i)th medium or inclusion at the y position, with $a_0 = 0$ and $\max(a_i) = h$ (Fig. 2). Note that we have omitted to write explicitly the dependences of \mathbf{A} , \mathbf{B} , \mathbf{C} on (i), but they do

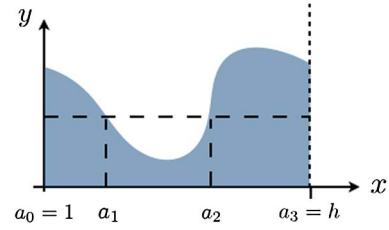


Fig. 2. Example of the local parametrization $a_i(y)$, here $i = 0, \dots, 3$.

depend on (i) because of their integral boundaries. More explicitly, we have

$$\begin{aligned} \mathbf{A}_{nm}(y) &= (a_{i+1} - a_i)/h, \\ \mathbf{A}_{nm}(y) &= \frac{e^{2i\pi(m-n)a_{i+1}/h} - e^{2i\pi(m-n)a_i/h}}{2i\pi(m-n)}, \quad n \neq m, \end{aligned} \quad (11)$$

and it follows that

$$\mathbf{B} = \mathbf{A}\Gamma, \quad \text{and} \quad \mathbf{C} = -\Gamma\mathbf{A}\Gamma, \quad \text{with } \Gamma = \text{diag}(i\gamma_n). \quad (12)$$

Although convolution of the Fourier transformers of two functions have not been used (and, thus, the factorization rules for the Fourier transform of the product of two functions are not questioned), the projections used in the weak formulation make the Toeplitz matrices appear. Indeed, it is easy to see that, for any field $g(x, y)$ (g being for instance the permeability),

$$\sum_i g \mathbf{A} = [g], \quad \text{with } [g]_{nm} \equiv \frac{1}{h} \int_0^h dx g(x, y) e^{2i\pi(m-n)x/h}. \quad (13)$$

Inspecting Eq. (9), it is convenient to rewrite the system by introducing an auxiliary field with modal components E_m to obtain a coupled system of the first ordinary differential equations:

$$\begin{aligned} E_n &\equiv [\varepsilon_{yy}^{-1}]_{nm} H_m' + i\gamma_n [\varepsilon_{xy}^{-1}]_{nm} H_m \\ E_n' + i\gamma_n [\varepsilon_{xy}^{-1}]_{nm} H_m' + (i\gamma_n)(i\gamma_m) [\varepsilon_{xx}^{-1}]_{nm} H_m + k^2 [\mu]_{nm} H_m &= 0, \end{aligned} \quad (14)$$

which we express in a matrix form for the two vectors composed by the modal components $\mathbf{E} \equiv (E_m)$ and $\mathbf{H} \equiv (H_m)$:

$$\begin{pmatrix} [\varepsilon_{yy}^{-1}] & 0 \\ \Gamma[\varepsilon_{xy}^{-1}] & \mathbf{I} \end{pmatrix} \begin{pmatrix} \mathbf{H} \\ \mathbf{E} \end{pmatrix}' = \begin{pmatrix} -[\varepsilon_{xy}^{-1}]\Gamma & \mathbf{I} \\ -\Gamma[\varepsilon_{xx}^{-1}]\Gamma - k^2[\mu] & 0 \end{pmatrix} \begin{pmatrix} \mathbf{H} \\ \mathbf{E} \end{pmatrix}, \quad (15)$$

where all the matrices and vectors are defined locally at y .

C. Energy Conservation

The energy flux across the section at any y position is defined by

$$\Phi(y) = -\frac{1}{2} \text{Re} \left[\int dx \tilde{E}_x H \right] = \frac{1}{2k} \text{Im} [{}^t \mathbf{E} \mathbf{H}], \quad (16)$$

from which $\partial_y \Phi = 1/(2k) \text{Im} [{}^t \mathbf{E}' \mathbf{H} + {}^t \mathbf{E} \mathbf{H}']$. The above system in Eq. (15) can be written as

$$\begin{pmatrix} \mathbf{H} \\ \mathbf{E} \end{pmatrix}' = \begin{pmatrix} \mathbf{M}_1 & \mathbf{M}_2 \\ \mathbf{M}_3 & \mathbf{M}_4 \end{pmatrix} \begin{pmatrix} \mathbf{H} \\ \mathbf{E} \end{pmatrix}, \quad (17)$$

with

$$\begin{cases} \mathbf{M}_1 \equiv -[\varepsilon_{yy}^{-1}]^{-1}[\varepsilon_{xy}^{-1}]\Gamma, \\ \mathbf{M}_2 \equiv [\varepsilon_{yy}^{-1}]^{-1}, \\ \mathbf{M}_3 \equiv \Gamma([\varepsilon_{xy}^{-1}][\varepsilon_{yy}^{-1}]^{-1}[\varepsilon_{xy}^{-1}] - [\varepsilon_{xx}^{-1}])\Gamma - k^2[\mu], \\ \mathbf{M}_4 \equiv -\Gamma[\varepsilon_{xy}^{-1}][\varepsilon_{yy}^{-1}]^{-1}. \end{cases} \quad (18)$$

Thus, we obtain

$$\partial_y \Phi = \frac{1}{2k} \text{Im} [{}^t \mathbf{H}' \mathbf{M}_3 \tilde{\mathbf{H}} + {}^t \mathbf{E} \tilde{\mathbf{M}}_2 \tilde{\mathbf{E}} + {}^t \mathbf{E} (\mathbf{M}_4 + {}^t \tilde{\mathbf{M}}_1) \tilde{\mathbf{H}}]. \quad (19)$$

In the case where the media are lossless ($(\varepsilon_X^{-1}, \varepsilon_Y^{-1})$ and μ are real), the Toeplitz matrices are self-adjoint and ${}^t \tilde{\Gamma} = -\Gamma$; thus, $\mathbf{M}_4 = -{}^t \tilde{\mathbf{M}}_1$, and we obtain

$$\partial_y \Phi = \frac{1}{4k} [{}^t \mathbf{H} ({}^t \mathbf{M}_3 - \tilde{\mathbf{M}}_3) \tilde{\mathbf{H}} + {}^t \mathbf{E} (\tilde{\mathbf{M}}_2 - {}^t \mathbf{M}_2) \tilde{\mathbf{E}}]. \quad (20)$$

With \mathbf{M}_2 and \mathbf{M}_3 being self-adjoint matrices, the variation of the energy flux vanishes $\partial_y \Phi = 0$, which shows that our formulation ensures the energy conservation (see also [27]).

3. NUMERICAL RESOLUTION

The modal system, Eq. (15), can be solved using several numerical schemes. We use one scheme of Magnus type, based on an impedance matrix, which links the vectors \mathbf{E} and \mathbf{H} :

$$\mathbf{E} = \mathbf{Y} \mathbf{H}. \quad (21)$$

The matrix \mathbf{Y} satisfies a Riccati equation, from Eq. (17),

$$\mathbf{Y}' = -\mathbf{Y} \mathbf{M}_2 \mathbf{Y} - \mathbf{Y} \mathbf{M}_1 - {}^t \tilde{\mathbf{M}}_1 \mathbf{Y} + \mathbf{M}_3, \quad (22)$$

which is similar to the one obtained in [27] for isotropic media and in [17] for stratified anisotropic media. To properly integrate the Riccati equation, one has to define the outgoing and ingoing waves, which is, in general, quite involved for anisotropic media [30,31]. As it is not the subject of the present paper, we consider only real values of the permittivities and permeabilities, for which no complications occur [Section 3.A leading to Eq. (25)]. This allows us to translate the radiation condition (at $y = 0$ in Fig. 3) as an initial value of the impedance Y_o (Section 3.B); afterward, the system is integrated using a Magnus scheme toward the entrance of the scattering region ($y = \ell_y$). This first integration gives the scattering matrix associated to the scattering region. When needed, the wavefield associated to a particular source term (incident wave) can be calculated by integrating the same system from $y = \ell_y$ to $y = 0$, using the impedance matrices previously computed (Section 3.C). The Magnus scheme has been presented elsewhere [27,32,33], and we collect in Appendix B the principle of the implementation.

A. Mode Selection

The two media at the entrance ($y \geq \ell_y$) and at the outlet ($y \leq 0$) being homogeneous, we have $a_0(y) = 0$ and $a_1(y) = b$. This implies $[g] = g\mathbf{1}$, and the matrices in Eqs. (17) and (18) simplify in

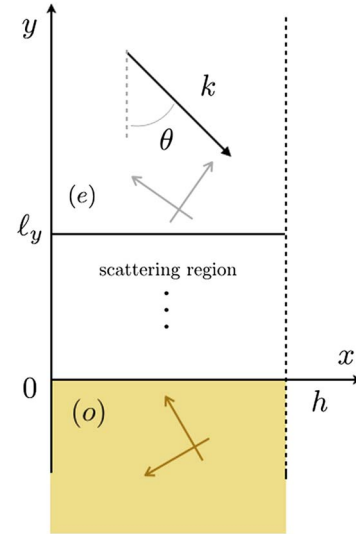


Fig. 3. Regions defined in the numerical scheme: (e) is the entrance medium, $y \geq \ell_y$, where the source is defined (here an incident plane wave) and (o) the outlet region $y \leq 0$. Both (o) and (e) can be anisotropic. In between, the scattering region contains anisotropic inclusions and/or anisotropic layers, and it corresponds to the domain where the numerical calculations is performed.

$$\begin{cases} \mathbf{M}_1 = \mathbf{M}_4 = -\frac{\varepsilon_{yy}}{\varepsilon_{xy}} \Gamma, \\ \mathbf{M}_2 = \varepsilon_{yy} \mathbf{1}, \\ \mathbf{M}_3 = \left(\frac{\varepsilon_{yy}}{\varepsilon_{xy}} - \frac{1}{\varepsilon_{xx}} \right) \Gamma^2 - k^2 \mu \mathbf{1} = -\frac{\varepsilon_{yy}}{\varepsilon_X \varepsilon_Y} \Gamma^2 - k^2 \mu \mathbf{1}, \end{cases} \quad (23)$$

where we used $\varepsilon_{yy}^{-1} \varepsilon_{xx}^{-1} - \varepsilon_{xy}^{-2} = \varepsilon_X^{-1} \varepsilon_Y^{-1}$. The second order equation on the (decoupled) modal components H_n simplifies in

$$\varepsilon_{yy}^{-1} H_n'' + 2i\gamma_n \varepsilon_{xy}^{-1} H_n' + (\mu k^2 - \gamma_n^2 \varepsilon_{xx}^{-1}) H_n = 0. \quad (24)$$

The waves propagating in such medium are of the form $e^{ikx + ik_n^\pm y}$, with the associated dispersion relation:

$$k_n^\pm = -\gamma_n \frac{\varepsilon_{yy}}{\varepsilon_{xy}} \pm \sqrt{\mu \varepsilon_{yy} k^2 - \gamma_n^2 \frac{\varepsilon_{yy}^2}{\varepsilon_X \varepsilon_Y}}. \quad (25)$$

The link between the above dispersion relation and the usual dispersion relation of birefringent media (expressed in the frame of the principal directions) is given in Appendix C. In the following, we define

$$\begin{aligned} \mathbf{K}^\pm &\equiv \varepsilon_{yy} [-\varepsilon_{xy}^{-1} \Gamma \pm \Delta], \\ \text{with } \Delta &\equiv i \varepsilon_{yy}^{-1} \sqrt{\mu \varepsilon_{yy} k^2 + \varepsilon_{yy}^2 \varepsilon_X^{-1} \varepsilon_Y^{-1} \Gamma^2}, \end{aligned} \quad (26)$$

the diagonal matrix with diagonal elements ik_n^\pm (a useful relation is $\varepsilon_{yy}^{-1} \mathbf{K}^\pm + \varepsilon_{xy}^{-1} \Gamma = \pm \Delta$).

Note that the notation k_n^\pm refers to waves propagating in the y direction (sign $+$) and to waves propagating in the $(-y)$ directions (sign $-$) only for nondissipative lossless media; in general, the distinction between both is involved and needs more careful criteria [30,31]. Here, it is easy to see that the flux of the Poynting vector $\Pi = \mathbf{E} \times \mathbf{H}$ across a section at constant y for a single mode k_n^\pm is

$$\begin{aligned}\Phi(k_n^\pm) &= \int \Pi \cdot d\mathbf{S} \\ &= \pm \frac{1}{2k} \operatorname{Re} \left[\varepsilon_{yy}^{-1} \sqrt{\mu \varepsilon_{yy} k^2 - \gamma_n^2 \varepsilon_{yy}^2} / \varepsilon_X \varepsilon_Y H_n \bar{H}_n \right], \quad (27)\end{aligned}$$

and $\Phi > 0$ means that the wave $e^{ik_x x + ik_n^\pm y}$ propagates in the y direction. We can distinguish two cases for real values of $(\varepsilon_X, \varepsilon_Y)$ and $\mu > 0$ (negative indices are disregarded).

- For positive permittivity parameters, the mode is propagating if $k^2 > \gamma_n^2 \varepsilon_{yy} / (\mu \varepsilon_X \varepsilon_Y)$, evanescent otherwise, and the sign \pm of k_n^\pm in Eq. (25) refers to the direction of propagation of the modes; for propagating modes because $\Phi(k_n^+) > 0$ and $\Phi(k_n^-) < 0$; for evanescent modes because the wave has to decrease in amplitude when propagates.

- For negative permittivity parameters, the modes are all evanescent, with $\Phi = 0$ (even if the k_n^\pm can have a real part); again, the sign \pm of k_n^\pm in Eq. (25) correctly refers to the direction of propagation of the modes.

B. Radiation Condition

The decoupled system for (\mathbf{E}, \mathbf{H}) in the region $y \leq 0$ is, from Eq. (17) and Eq. (23),

$$\mathbf{E} = \varepsilon_{yy}^{-1} \mathbf{H}' + \varepsilon_{xy}^{-1} \Gamma \mathbf{H}, \quad \mathbf{E}' = \varepsilon_{yy} [\Delta_o^2 \mathbf{H} - \varepsilon_{xy}^{-1} \Gamma \mathbf{E}]. \quad (28)$$

The waves transmitted in the outlet region are moving away from the interface $y = 0$ [along the $(-y)$ direction]. Thus, they satisfy $H'_n = ik_n^- H_n$ (namely, $E'_n = ik_n^- E_n$), which leads to $\mathbf{E} = -\Delta_o \mathbf{H}$, and the impedance matrix is, from Eq. (21),

$$\mathbf{Y}_o = -\Delta_o, \quad (29)$$

where Δ_o is defined in Eq. (26), with the characteristics $(\varepsilon_{xx}, \varepsilon_X, \varepsilon_Y) = (\varepsilon_{xx}, \varepsilon_X, \varepsilon_Y)_o$ and $\mu = \mu_o$ of the medium (o). Alternatively, it is easy to see that \mathbf{Y}_o is one (constant) solution of the Riccati equation, Eq. (22), with $\mathbf{M}_3 = -\varepsilon_{yy} \Delta_o^2$ and

$$\mathbf{Y}' = -\varepsilon_{yy} [\mathbf{Y}^2 - \Delta_o^2], \quad (30)$$

and the proper sign is given by the condition of outgoing waves.

Starting from the initial value $\mathbf{Y}(0) = \mathbf{Y}_o$, the differential system in Eq. (22) can be integrated using a Magnus scheme, as described in Appendix B. In the following, we denote \mathbf{Y}_e the computed impedance matrix, $\mathbf{Y}(\ell_y) = \mathbf{Y}_e$.

C. Source Term

We consider any source in (e) being a superposition of waves propagating in the $(-y)$ direction: $H_n^i \propto e^{ik_n^i y + ik_x x}$, where the k_n^\pm is defined in Eq. (25) with $(\varepsilon_{xx}, \varepsilon_X, \varepsilon_Y) = (\varepsilon_{xx}, \varepsilon_X, \varepsilon_Y)_e$ and $\mu = \mu_e$. Then, the reflected field is a superposition of waves propagating in the $+y$ direction, $H_n^r \propto e^{ik_n^r y + ik_x x}$. The reflection matrix \mathbf{R} is defined for the vectors of modal components $\mathbf{H}^r = \mathbf{R} \mathbf{H}^i$. With \mathbf{K}_e^\pm being defined in Eq. (26) in (e), we have for the total field $\mathbf{H} = \mathbf{H}^i + \mathbf{H}^r$

$$\mathbf{H}' = (\mathbf{K}_e^- + \mathbf{K}_e^+ \mathbf{R}) \mathbf{H}^i. \quad (31)$$

Using the relation $\mathbf{H}' = [\varepsilon_{yy} (\mathbf{E} - \varepsilon_{xy}^{-1} \Gamma \mathbf{H})]_e$, we obtain $(\mathbf{K}_e^- + \mathbf{K}_e^+ \mathbf{R}) = \varepsilon_{yy} (\mathbf{I} + \mathbf{R}) (\mathbf{Y}_e + \varepsilon_{xy}^{-1} \Gamma)$ and eventually

$$\mathbf{R} = [\Delta_e - \mathbf{Y}_e]^{-1} [\Delta_e + \mathbf{Y}_e]. \quad (32)$$

In the simplest case, where (e) is made of isotropic material ($\varepsilon_{yy}^{-1} = \varepsilon_{xx}^{-1} = 1/\varepsilon$, $\varepsilon_{xy}^{-1} = 0$, and $\Delta_e = -\mathbf{K}$), we recover $\mathbf{R} = [\mathbf{K} + \mathbf{Y}_e]^{-1} [\mathbf{K} - \mathbf{Y}_e]$, as in [27].

D. Validation for a Single Interface between Two Anisotropic Media

As a basic validation, we derive the Fresnel coefficients in the case of a single interface at $y = 0$ between two anisotropic media (Fig. 4). In this case, no mode conversion occurs, and the problem can be solved easily for an incident plane wave hitting the interface at incidence θ ($\kappa = k \sin \theta$), leading to

$$\begin{cases} H(x, y < 0) = e^{ik \sin \theta x} [e^{ik_e y} + R e^{ik_e^+ y}], \\ H(x, y \geq 0) = e^{ik \sin \theta x} T e^{ik_o y}. \end{cases} \quad (33)$$

The wavenumber k_e^\pm (namely, k_o^\pm) satisfies the dispersion relation $\varepsilon_{yy}^{-1} (k^\pm)^2 + 2\varepsilon_{xy}^{-1} \kappa k^\pm + (\varepsilon_{xx}^{-1} \kappa^2 - \mu k^2) = 0$, leading to

$$\begin{aligned} k^\pm &= \varepsilon_{yy} k (-\varepsilon_{xy}^{-1} \sin \theta \pm \delta), \\ \text{with } \delta &\equiv \sqrt{\mu \varepsilon_{yy}^{-1} - \varepsilon_X^{-1} \varepsilon_Y^{-1} \sin^2 \theta}, \end{aligned} \quad (34)$$

which applies for k_e^\pm and for k_o^\pm . Obviously, this coincides with the expression of k_n^\pm with $n = 0$ in Eq. (25), since the present problem involves the mode 0 only. Applying the continuity of H and of $\varepsilon_{xy}^{-1} \partial_x H + \varepsilon_{xx}^{-1} \partial_y H$ at the interface $y = 0$ leads to the expression of the reflection coefficient R :

$$R = \frac{\delta_e - \delta_o}{\delta_e + \delta_o}. \quad (35)$$

In [34], the reflection coefficient for an interface between air at $y > 0$ and an anisotropic medium with $\mu = 1$ and $\alpha = 0$ is derived; in that case, our expression simplifies with $\mu_e = 1$ leading to $\delta_e = \cos \theta$ and $(\mu_o = 1, \varepsilon_{yy,o} = \varepsilon_X)$, leading to

$$R(\text{air}, \alpha = 0) = \frac{\cos \theta - \sqrt{\varepsilon_X^{-1} - \varepsilon_X^{-1} \varepsilon_Y^{-1} \sin^2 \theta}}{\cos \theta + \sqrt{\varepsilon_X^{-1} - \varepsilon_X^{-1} \varepsilon_Y^{-1} \sin^2 \theta}}, \quad (36)$$

which is in agreement with Eq. (7) in [34]. Also, coming back to the general case, we obtain, from Eq. (35), a generalization of the Brewster angle, realizing perfect transmission ($\delta_e = \delta_o$):

$$\theta_B = \operatorname{asin} \sqrt{\frac{\varepsilon_X \varepsilon_Y}{\varepsilon_{yy}} \frac{\varepsilon_{yy} - 1}{\varepsilon_X \varepsilon_Y - 1}}, \quad (37)$$

which coincides with the result in [34] for $\alpha = 0$.

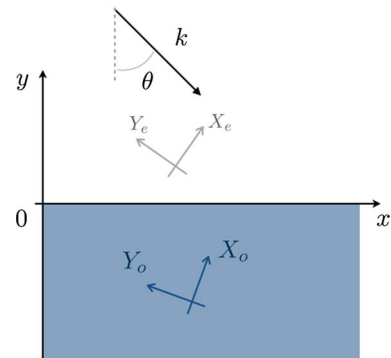


Fig. 4. Single interface between two anisotropic media.

Finally, it was our aim to check that this expression is consistent with our numerical scheme: Equations (34) and (26) show that $\Delta_{e,00} = ik\delta_e$ and $\Delta_{o,00} = ik\delta_o$. Thus, the reflection coefficient derived for a single interface R coincides with R_{00} , the reflection coefficient of the mode 0 for an incident wave in mode 0 of the reflection matrix \mathbf{R} in Eq. (32), as expected.

4. CONVERGENCE AND VALIDATION OF THE NUMERICAL METHOD

To validate our numerical method, we consider two different examples.

- First, the convergence of the method is inspected in a problem of scattering by arrays of anisotropic inclusions. Three different shapes of the inclusions are considered to inspect the sensitivity of our modal formulation to the problem of staircase approximation [28]. To anticipate, and, as already mentioned in a previous study [27], our formalism presents the same order of magnitude in the error and the same rate of convergence for various shapes, being piecewise constant or not, and this tends to prove that Li's rules are not questioned in our formalism.

- We also propose a validation of our method by comparison with direct calculations of the scattering by a subwavelength layered medium. Beyond the validation of our formalism, such calculations are of interest. Indeed, one source of interest in the anisotropic structures is its ability to describe the behavior of subwavelength layered media, invoking the theory of homogenization. When applicable, the numerical cost is obviously much lower since the microstructure has not been resolved. We inspect this equivalence between anisotropic media and layered media through the example of guided waves propagating in a guide made of dielectric slanted layers.

A. Convergence: Scattering by an Array of Anisotropic Inclusions of Various Shapes

As a first illustrative example, Fig. 5 shows the real part of the wave field $H(x, y)$, resulting from the interaction of an incident plane wave with an h periodic array of anisotropic discs of radius R . Calculations have been performed for $kR = 3$ and $kh = 10$, and a wave incident on the array with an angle $\theta = 45^\circ$ with the array. The discs are made of an anisotropic medium with $\epsilon_X = 1.9$ and $\epsilon_Y = 8.5$ [to fix the idea, this would correspond to the effective parameters of a medium made of layers alternating air $\epsilon = 1$ and dielectric material at $\epsilon = 16$ with equal filling fraction; see forthcoming Eq. (38)]. In the three configurations, everything is identical except the anisotropy direction, being given by α , ($\alpha = 0^\circ, 45^\circ$ and 90°); the effect of the anisotropy direction appears clearly.

Next, we inspect the convergence of the numerical scheme. To do this, we consider three shapes of anisotropic inclusions: the previous discs of radius R , rectangles of size $L \times \ell$ and inclusions with nuts shape parametrized by (a_1, a_2) [35]. For simplicity, we have chosen the same filling fraction $\varphi \simeq 0.3$ for the three shapes, being defined in a unit cell of size $h \times h$. Otherwise, we use the same anisotropic material ($\epsilon_X = 1.9$, $\epsilon_Y = 8.5$, $\mu = 1$), the same direction of anisotropy $\alpha = 20^\circ$, and we fix the incident wave properties: $k^2\varphi \simeq 28.3$ (see the figure caption for a complete description of the inclusion shape)

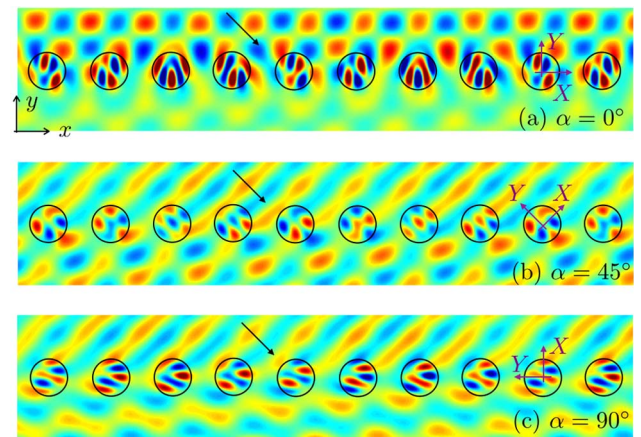


Fig. 5. Real part of the wave fields $H(x, y)$ computed for arrays of anisotropic discs h spaced ($\epsilon_X = 1.9$, $\epsilon_Y = 8.5$) with principal directions (X, Y) tilted through an angle α . The incident wave, with $kh = 10$, $kR = 3$, hits the array at angle $\theta = 45^\circ$. The arrays in the three plots have the same properties except the anisotropy angle: (a) $\alpha = 0^\circ$, (b) $\alpha = 45^\circ$, and (c) $\alpha = 90^\circ$.

and $\theta = 0^\circ$ or 45° . Figure 6 shows the wave fields for $\theta = 0^\circ$. We used a truncation order $N = 20$ in the numerical computations, and no significant variation of the wavefield is observed for higher truncation orders.

Figure 7 illustrates further the convergence of the method. We report the reflection coefficient R as a function of the truncation order N (main plot) and the rate of convergence (inset), measured as the difference between R for a truncation at varying N and a converged version of $R(N \rightarrow \infty)$ (obtained in the practice for $N = 200$). At this frequency ($kh = 10$), three modes are propagating in the air, and in the anisotropic inclusions, four modes (for $\theta = 0^\circ$) or five modes (for $\theta = 45^\circ$) are propagating. The reflection coefficients reach a merely constant value for $N = 50$ independently of the shape of the inclusion. More quantitatively, it can be seen in the inset of Fig. 7 that the error is less than 2% for $N > 10$, 1% for $N > 40$. The rate of convergence is roughly $1/N^{3/2}$ (dotted line in the inset of Fig. 7), which coincides with the expected rate of convergence for a wave field having discontinuous gradient. Indeed, a general theorem on the modal series applies here: for a function that has a regularity given by a class C^m , the convergence of the error $E(N)$ on the series truncated at order N is $E \sim 1/N^s$, with $s < m + 3/2$ [36]. In the present case, H is of class C^0 , leading to a best convergence for $E \sim 1/N^{3/2}$.

In several papers, the staircase approximation has been regarded and identified as a possible reason for low convergence or, say at least, high errors. For not piecewise constant shapes, the convergence is restored if Li's rules, or Laurent's rules, have to be used to properly express the Fourier transform of a product of functions [25]. Our conclusion here is the same as in our previous studies concerning penetrable isotropic inclusions [27]: the order of magnitude of the error and the rate of convergence in our numerical scheme appear to be insensitive to the fact that the inclusion shapes are piecewise constant (as for the rectangular inclusion shape) or not (as for the circular shape and the nuts shape).

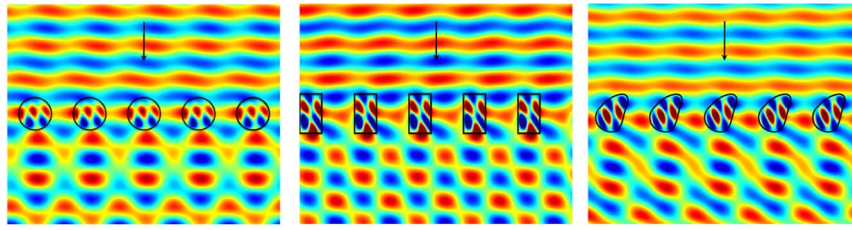


Fig. 6. Real part of the wave fields $H(x, y)$ computed for arrays of d spaced inclusions made of an anisotropic material ($\epsilon_X = 1.9, \epsilon_Y = 8.5$) with principal directions tilted through $\alpha = 20^\circ$. The incident wave hits the array at normal incidence ($\theta = 0$, black arrow) with $kb = 10$, and the shape of the inclusions is varied: (a) cylindrical inclusions, with radius R ($kR = 3$); (b) rectangular inclusion of size $L \times \ell$, ($kL = 7, k\ell = 4$); and (c) non-symmetrical shape (see text). The three shapes have the same filling fraction in a unit cell, $kh \times kb = 10 \times 10$.

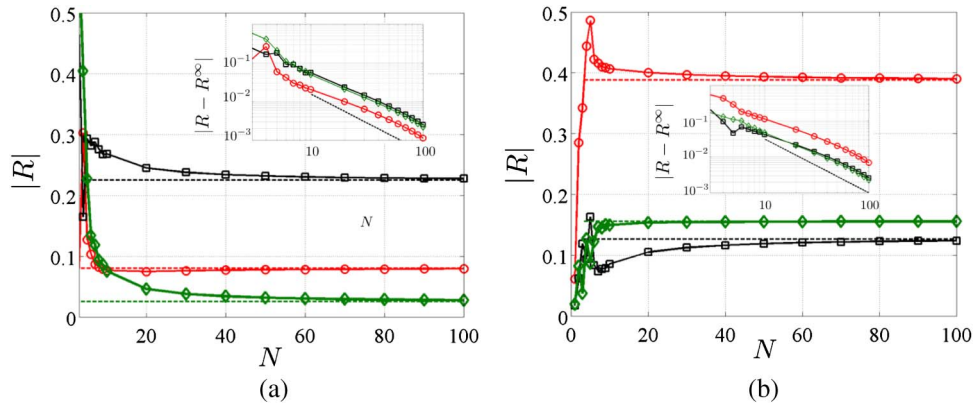


Fig. 7. Reflection coefficient $|R|$ of the mode 0 as a function of the truncation order N for the three shapes of Fig. 6, the discs (circle, red symbol), the rectangles (black rectangle symbols), and the nut shapes (green diamond), (a) for $\theta = 0$ and (b) for $\theta = 45^\circ$. The insets show the rate of convergence in log-log scale; $|R - R^\infty|$ as a function of N (in the practice calculated R^∞ is computed using $N = 200$). The dotted black lines indicated a $(-3/2)$ -slope.

B. Validation: Case of Guided Waves in an Effective Anisotropic Guide

In this section, we validate our numerical method by inspecting the equivalence between layered media and anisotropic media. According to the theory of layered media, subwavelength layers alternating materials with $\epsilon_{\ell 1}$ and $\epsilon_{\ell 2}$ [Fig. 8(a)] behave as an anisotropic medium [Fig. 8(b)] with characteristics

$$\epsilon_X = [\varphi/\epsilon_{\ell 1} + (1 - \varphi)/\epsilon_{\ell 2}]^{-1}, \quad \epsilon_Y = \varphi\epsilon_{\ell 1} + (1 - \varphi)\epsilon_{\ell 2}, \tag{38}$$

where (X, Y) are, respectively, the directions perpendicular and parallel to the layers and φ is the filling fraction of $\epsilon_{\ell 1}$ ($\varphi = 1/2$ for layers of equal width) [37].

We consider a guide of length ℓ containing slanted layers of equal width $d = 0.1\ell$ with a tilted angle $\alpha = 45^\circ$, alternating dielectric materials with $\epsilon_{\ell 1} = 100$ and $\epsilon_{\ell 2} = 2$ [Fig. 8(a)]. The layered guide is supported by a dielectric substrate with $\epsilon_2 = 2$, and the incident wave is sent in the air ($y > \ell$). We compute the reflection coefficient R_{ex} for an incident wave being characterized by (k, κ) , and the wave is evanescent for $\kappa > k$; it is propagating otherwise. For this calculation, the length $b \times H$ of the unit cell is imposed by the characteristics of the layers $b = d/\cos \alpha, H = d/\sin \alpha$. Then, it is repeated

periodically, and eventually truncated, until ℓ is reached (see Appendix D).

The reflection coefficient R_{ex} of the actual layered guide is compared to the one, denoted R_{anis} , computed for the equivalent anisotropic guide [Fig. 8(b)]. Results are reported in Fig. 8(c); we have fixed $\kappa\ell = 1.5$, and we have varied the frequency $k\ell \in [0, 3]$ ($kd \in [0, 0.3]$). The results are in excellent agreement in the whole range of explored frequencies.

To go further in the validation of our numerical scheme, we inspect the wave field of the wave guided within the waveguide and visible by means of a divergence of the reflection coefficients below the light line $k = \kappa$ [GW in Fig. 8(c), for $k\ell \simeq 0.85$]. This guided wave propagates along the x direction in the guide with a wavenumber κ ; otherwise, it is evanescent in the air and in the substrate. For the anisotropic guide, it is strictly a guided wave and for the layered guide, it is a sort of spoof plasmon for dielectric structured grating. These resonant waves are known to be sensitive to any variation of the refractive index in the surrounding media; thus, adding a perturbation in the layer of air is expected to destroy the resonance, and we inspect this aspect by adding an array of small dielectric nuts, with permittivity $\epsilon = 20$. Finally, to excite this resonant wave from outside, we choose a more realistic configuration in which we have added a layer at the entrance with permittivity

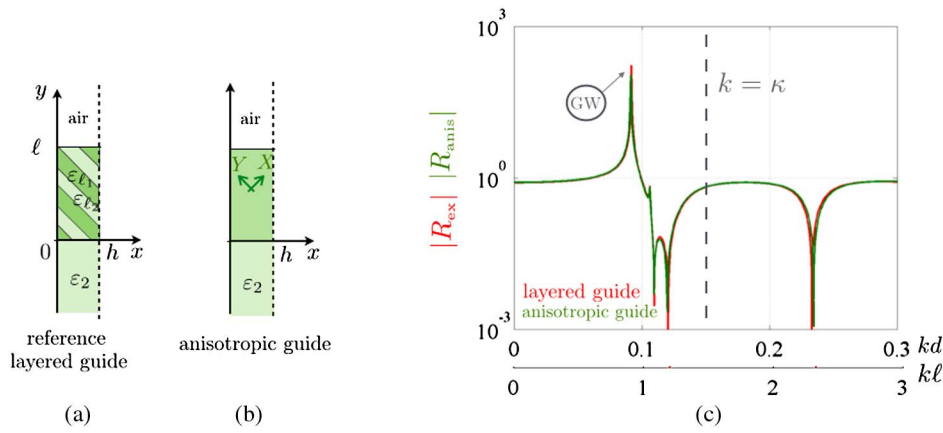


Fig. 8. (a) Layered guide of length ℓ with slanted layers of equal width $d = 0.1\ell$ ($\alpha = \pi/4$). (b) Equivalent homogeneous anisotropic guide with principal permittivities ϵ_X and ϵ_Y , Eq. (38). (c) Reflection coefficients $|R_{\text{ex}}|$ and $|R_{\text{anis}}|$ in the configurations (a) and (b), for $k\ell \in [0, 3]$. Below the light line $k = \kappa$, a guided wave (GW) is visible by means of a resonance in the reflection coefficients.

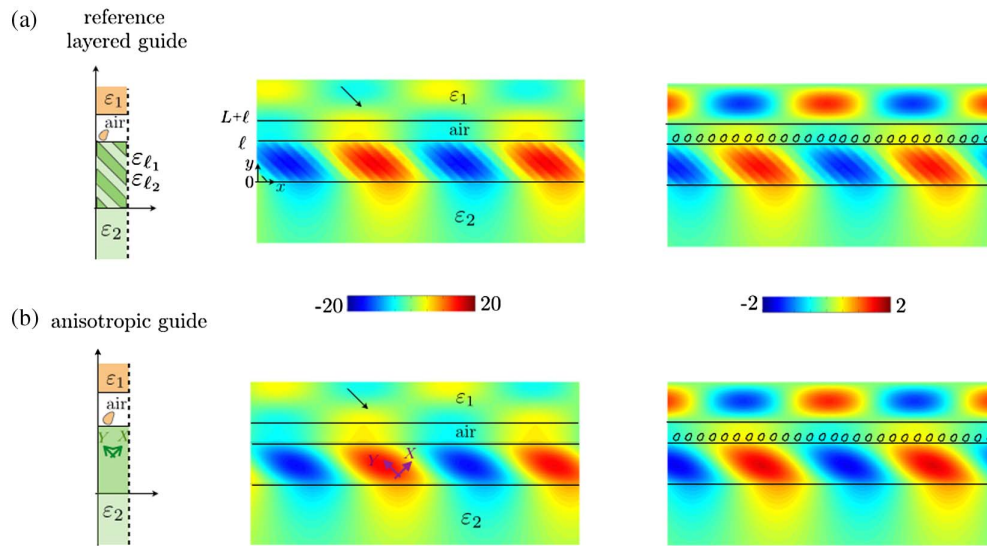


Fig. 9. Real parts of the wave fields $H(x, y)$ for the layered guide (see main text): (a) at the resonance frequency of the guided wave and (b) at the same frequency but inserting, as perturbation, an array of small inclusions. The layers are materialized by plain lines only on a part of the figure to let the fields be visible. (c) and (d) show the same calculation replacing the layered guide with an equivalent anisotropic guide.

$\epsilon_1 = 20$, such that the incident wave is propagating with incident angle $\theta \simeq 23^\circ$ in order to obtain $\kappa = k\sqrt{\epsilon_1} \sin \theta$ (and $k\ell \simeq 0.85$ for $\kappa\ell = 1.5$). The layer of air has a length $L = 0.5\ell$ in these calculations. The wave field patterns are shown in Fig. 9 for the guided waves (center panels) and for the guided wave perturbed by the array of dielectric nuts (right panels). In both cases, the agreement between the wave field patterns in the reference calculations and using our anisotropic calculations is excellent, although we observe in the reference calculations scars in the reference waveguide, which are due to the actual layers with finite (nonvanishing) width.

We have validated our numerical scheme for anisotropic structures by comparison with a reference microstructured medium with effective anisotropy, being known by the homogenization process. In addition to this validation, the

equivalence between structured media and effective anisotropic media is of interest in terms of numerical cost. Indeed, dealing with microstructured media presents two difficulties.

- First, the microstructure has to be captured, even roughly, which implies a sufficient truncation order N . Although this is not a heavy constraint in the presented cases ($N \sim 10$), it may become much heavier for more complex interface shapes.
- The length of the unit cell increases with α as $h = d / \cos \alpha$ (Appendix D). This is penalizing for a large α angle, since it produces an increasing number of propagating modes that have to be accounted for in the computation.

5. CONCLUSION

We have presented a multimodal method based on the use of the admittance matrix to describe the propagation of

electromagnetic waves in anisotropic periodic media, containing arbitrary-shaped anisotropic inclusions or anisotropic media with arbitrary-shaped interfaces, or both. Our coupled wave equations are based on a weak formulation, which avoids dealing with the Fourier transform of a product of functions and, thus, does not address Li's rules. Together with the local admittance formulation, it leads to an efficient and easily implementable numerical method, which is well suited to describe the continuously variable shape of scatter-

$$\boldsymbol{\epsilon} = \begin{pmatrix} \epsilon_{11} = \epsilon_X \cos^2 \alpha + \epsilon_Y \sin^2 \alpha & \epsilon_{12} = (\epsilon_X - \epsilon_Y) \cos \alpha \sin \alpha & 0 \\ \epsilon_{12} & \epsilon_{22} = \epsilon_X \sin^2 \alpha + \epsilon_Y \cos^2 \alpha & 0 \\ 0 & 0 & \epsilon_Z \end{pmatrix}. \quad (\text{A1})$$

ers, beyond the usual staircase approximation (the error, as the rate of convergence has been shown to be independent of the inclusion shape). The method has been shown to have good convergence for wave fields presenting discontinuous gradients, namely varying as $N^{-3/2}$, N being the truncation order in the modal expansion. A validation of our numerical method has been presented by comparison with a microstructured medium presenting an effective anisotropy at the wave scale.

In the present study, we have considered media with real permittivity and permeability and no spatial dispersion. These constraints are only motivated by the ease, for such material properties, in selecting right- and left-going waves, which is necessary to properly account for the radiation condition (Section 3.A). The extension of the presented method into more complex and more realistic material properties is straightforward if the problem of the selection of these waves is addressed.

In general, the modal methods can be applied quasi indifferently to the case of periodic arrays and to the case of waveguides (owing to a change in the modal basis). In the present case, we see an interesting limitation for the extension of our method to the case of waveguides with perfectly conducting walls. Indeed, the nice property in which the modal system is decoupled outside the scattering region relies on the choice of the modal basis $\varphi_m(x)$: the expansion of H on the φ_m has to satisfy the boundary condition at $x = 0, h$ for any truncation outside the scattering region. This is needed to properly define the initial value of the impedance matrix, or in other words, to properly select the modes propagating away from the scattering region; if not the case, the method fails. The situation is different if the boundary conditions are not satisfied inside the scattering region; in this case, the convergence is altered, but the modal method still holds. In the present case, the condition of pseudo-periodicity is satisfied by $\varphi_m(x)$ and by $\varphi'_m(x)$; this ensures that the expansion of H satisfies the right boundary condition. In perfectly conducting waveguides, Neumann boundary conditions apply. For isotropic media, only vanishing first derivatives of the basis functions are needed, which is obtained using the usual cosine functions. For anisotropic media, this would require

vanishing values of the functions and the first derivatives. The problem being identified, it should be possible to find a new basis with such properties. Works are in progress in this direction.

APPENDIX A: PERMITTIVITY TENSOR

In our formulation, Eq. (1), $\mathbf{D} = \boldsymbol{\epsilon}\mathbf{E}$ with $\boldsymbol{\epsilon}$ expressed in the frame (x, y) :

For TM waves, \mathbf{E} and \mathbf{D} are in plane vectors ($E_z = D_z = 0$) associated to the permittivity tensor in 2D:

$$\boldsymbol{\epsilon} \equiv \begin{pmatrix} \epsilon_{11} & \epsilon_{12} \\ \epsilon_{12} & \epsilon_{22} \end{pmatrix}. \quad (\text{A2})$$

Our notations for ϵ_{ij}^{-1} (i, j are x or y) in Eqs. (4) are linked to the usual ϵ_{ij} (i, j are 1 or 2) in the permittivity tensor by

$$\begin{pmatrix} \epsilon_{xx}^{-1} & \epsilon_{xy}^{-1} \\ \epsilon_{xy}^{-1} & \epsilon_{yy}^{-1} \end{pmatrix} = \frac{1}{\det(\boldsymbol{\epsilon})} \boldsymbol{\epsilon}, \quad (\text{A3})$$

with $\det(\boldsymbol{\epsilon}) = \epsilon_X \epsilon_Y$ (or $\epsilon_{ij}^{-1} = \epsilon_{ij}/(\epsilon_X \epsilon_Y)$). Equation (2) reads

$$\nabla \cdot \left[\frac{1}{\det(\boldsymbol{\epsilon})} \boldsymbol{\epsilon} \nabla H \right] + k^2 \mu H = 0. \quad (\text{A4})$$

APPENDIX B: INTEGRATION OF THE RICCATI EQUATION; MAGNUS SCHEME

The integration of the modal system [Eq. (17)] requires care. First, contamination by exponentially growing evanescent modes has to be avoided. Second, the original problem is posed as a boundary value problem, with a forcing source at $y = \ell_y$ and a radiation condition at $y = 0$. Therefore, the coupled first-order in Eq. (17) cannot be solved directly as an initial value problem. To circumvent these problems, we implement a multimodal admittance method, which leads to a stable initial value problem (see Fig. 10).

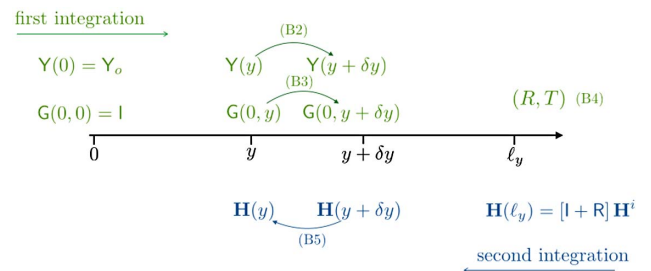


Fig. 10. Illustration of the numerical scheme.

1. Computation of the Scattering Matrices

Starting from an initial condition $Y(0) = Y_o$, the admittance matrix is calculated, following the scheme in Eq. (17) written as a system:

$$\mathbf{F}(y)' = \mathbf{M}(y)\mathbf{F}(y), \quad \text{with } \mathbf{F} \equiv \begin{pmatrix} \mathbf{H} \\ \mathbf{E} \end{pmatrix},$$

$$\mathbf{M} = \begin{pmatrix} \mathbf{M}_1 & \mathbf{M}_2 \\ \mathbf{M}_3 & \mathbf{M}_4 \end{pmatrix}.$$

This evolution equation can be solved using a Magnus scheme. With a given discretization along y with step δy , the solution at $y + \delta y$ is given from the solution at y using the matrix exponential $\mathbf{N} \equiv e^{\mathbf{M}(y+\delta y/2)\delta y}$ defined at the middle position between both; then

$$\mathbf{F}(y + \delta y) = \mathbf{N}\mathbf{F}(y), \quad \text{and we denote } \mathbf{N} \equiv \begin{pmatrix} \mathbf{N}_1 & \mathbf{N}_2 \\ \mathbf{N}_3 & \mathbf{N}_4 \end{pmatrix}. \quad (\text{B1})$$

$\mathbf{F}(0)$ is unknown, but $Y(0)$ is known, and the above equation can be used to find $Y(y)$:

$$Y(y + \delta y) = [\mathbf{N}_3 + \mathbf{N}_4 Y(y)][\mathbf{N}_1 + \mathbf{N}_2 Y(y)]^{-1},$$

$$Y(0) = Y_o, \quad (\text{B2})$$

which is used from $y = 0$ (Y_o is known from the radiation condition) to $y = \ell_y$. Together with the computation of Y , one computes the propagator \mathbf{G} defined as

$$\mathbf{H}(0) = \mathbf{G}(0, y)\mathbf{H}(y), \quad \text{which satisfies}$$

$$\mathbf{G}(0, y + \delta y)\mathbf{H}(y + \delta y) = \mathbf{G}(0, y)\mathbf{H}(y) \text{ with } \mathbf{G}(0, 0) = \mathbf{I}$$

This allows us to compute \mathbf{G} together with Y :

$$\mathbf{G}(0, y + \delta y) = \mathbf{G}(0, y)[\mathbf{N}_1 + \mathbf{N}_2 Y(y)]^{-1}, \quad \mathbf{G}(0, 0) = \mathbf{I}. \quad (\text{B3})$$

(Incidentally, note that \mathbf{G} satisfies also a Riccati equation $\mathbf{G}' = -\mathbf{G}[\mathbf{M}_1 + \mathbf{M}_2 Y]$.)

The calculation of Y and \mathbf{G} allows us to obtain the scattering properties of the region $\{(x, y) \in [0, b] \times [0, \ell_y]\}$ in terms of the reflection matrix \mathbf{R} and transmission matrix \mathbf{T} :

$$\begin{cases} \mathbf{R} = [\Delta_e - Y(\ell_y)]^{-1}[\Delta_e + Y(\ell_y)], & \text{with } \mathbf{H}(\ell_y) = [\mathbf{I} + \mathbf{R}]\mathbf{H}^i, \\ \mathbf{T} = \mathbf{G}(0, \ell_y)[\mathbf{I} + \mathbf{R}], & \text{with } \mathbf{H}(0) = \mathbf{T}\mathbf{H}^i, \end{cases} \quad (\text{B4})$$

for any incident wave \mathbf{H}^i . Note that the computations of \mathbf{R} and \mathbf{T} do not require any storage of Y and \mathbf{G} along the y axis.

2. Computation of the Wave Field for a Given Source Term

If the wave field resulting from a given source term \mathbf{H}^i is regarded, it is sufficient to store the $Y(y)$ values in the first integration (from $y = 0$ to $y = \ell_y$); afterward, the forward integration (along $-y$) can be done. In this case, $\mathbf{H}(\ell_y) = [\mathbf{I} + \mathbf{R}]\mathbf{H}^i$ being known, we use the formulation on \mathbf{F} in Eq. (B1) to obtain

$$\mathbf{H}(y) = [\mathbf{N}_1 + \mathbf{N}_2 Y(y)]^{-1} \mathbf{H}(y + \delta y). \quad (\text{B5})$$

3. Remark on the Discretization δy along the y Axis

Because the exponential matrix involves real and imaginary terms of the matrix \mathbf{M} , δy has to be chosen to ensure nondiverging terms. This is usually done by imposing δy equal to the inverse of the wavenumber associated to the most evanescent mode. This is consistent with the physical argument that the spatial discretization has to resolve the smallest scale associated to the spatial variations in the wave field. As a rough estimate, the evanescent modes are associated to the scales $b/(n\pi)$, with $n \leq N$, N being the truncation order. Without further investigation of possible smaller scales in the other materials, one must have

$$\delta y \leq \frac{b}{N\pi}. \quad (\text{B6})$$

It can be noted, for instance, in [38] that numerical instabilities occur for the increasing value of N (the discretization being fixed to $\delta y/b = 1/30$, instabilities are observed for $12 < N < 25$, which do not appear for $\delta y/b = 1/100$). We believe this may be attributable to the step size, which is not adapted to the truncation. Nevertheless, note that it also may be questionable to increase the number of modes if the discretization becomes unable to inspect the corresponding spatial variations.

APPENDIX C: IN PLANE BIREFRINGENCE

We have expressed the wavenumber along y in the frame (x, y) tilted through α with respect to the frame of the principal direction of anisotropy (X, Y) , Eq. (25). From Eq. (24), written with $n = 0$ ($\gamma_n = \kappa$, the component of the wave vector along x), we obtain

$$\epsilon_{yy}^{-1} k_y^2 + 2\kappa \epsilon_{xy}^{-1} k_y + (\kappa^2 \epsilon_{xx}^{-1} - \mu k^2) = 0. \quad (\text{C1})$$

When expressed in the (X, Y) , the wave vector has components $\mathbf{k} = (k_X, k_Y)$, with

$$\begin{cases} \kappa = \cos \alpha k_X + \sin \alpha k_Y, \\ k_y = -\sin \alpha k_X + \cos \alpha k_Y, \end{cases} \quad (\text{C2})$$

from which we deduce, using Eqs. (4), the dispersion relation expressed in terms of (k_X, k_Y) :

$$\epsilon_X k_X^2 + \epsilon_Y k_Y^2 = \mu \epsilon_X \epsilon_Y k^2. \quad (\text{C3})$$

This is the usual form of the dispersion relation for birefringent medium (if, for instance, $\epsilon_Z = \epsilon_X$), restricted here to in-plane incidences, which defines the surface of the indices.

APPENDIX D: PARAMETRIZATION OF LAYERED MEDIA

To parametrize the layered structure, we define the unit cell, which can be replicated periodically along x and y . The cell has the size $b = d/\cos \alpha$ along x , $b/\tan \alpha = d/\sin \alpha$ along y , and the unit cell contains three slanted layers. At each y value, the a_n is given by the lines $x_i(y)$ ($i = 1, \dots, 4$), as shown in Fig. 11 (and $a_0 = 0$, $\max(a_n) = 1$); finally, depending on the α value, we may have four a_n values (for low α value, as in the presented case) or between four and five a_n values (for high α value). With

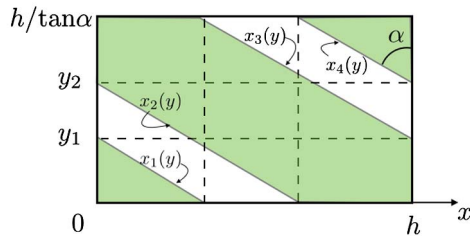


Fig. 11. Example of the local parametrization $a_i(y)$, here $i = 0, \dots, 3$.

$$y_1 = \frac{1 - \varphi}{2 \sin \alpha} d, \quad y_2 = \frac{1 + \varphi}{2 \sin \alpha} d, \quad (D1)$$

the four lines are given by

$$\begin{cases} 0 \leq y \leq y_1, & x_1(y) = \frac{(1-\varphi)d}{2 \cos \alpha} - y \tan \alpha, \\ 0 \leq y \leq y_2, & x_2(y) = \frac{(1+\varphi)d}{2 \cos \alpha} - y \tan \alpha, \\ y_1 \leq y \leq d/\sin \alpha, & x_3(y) = \frac{(3-\varphi)d}{2 \cos \alpha} - y \tan \alpha, \\ y_2 \leq y \leq d/\sin \alpha, & x_4(y) = \frac{(3+\varphi)d}{2 \cos \alpha} - y \tan \alpha \end{cases} \quad (D2)$$

Then, the cell can be repeated by shifting the unit cell along y , $y = 0 \rightarrow y = d/\sin \alpha$.

Centre National de la Recherche Scientifique (CNRS).

A. M. thanks the support of LABEX WIFI (Laboratory of Excellence within the French Program Investments for the Future) under references ANR-10-LABX-24 and ANR-10-IDEX-0001-02 PSL*.

REFERENCES AND NOTES

1. S. Brugioni and R. Meucci, "Characterization of a nematic liquid crystal light modulator for mid-infrared applications," *Opt. Commun.* **216**, 453–458 (2003).
2. H. Ren and S. T. Wu, "Anisotropic liquid crystal gels for switchable polarizers and displays," *Appl. Phys. Lett.* **81**, 1432–1434 (2002).
3. C. Y. Chen, C. L. Pan, C. F. Hsieh, Y. F. Lin, and R. P. Pan, "Liquid-crystal-based terahertz tunable Lyot filter," *Appl. Phys. Lett.* **88**, 101107 (2006).
4. P. K. Choudhury and W. K. Soon, "On the tapered optical fibers with radially anisotropic liquid crystal clad," *Prog. Electromagn. Res.* **115**, 461–475 (2011).
5. N. Singh, A. Tuniz, R. Lwin, S. Atakaramians, A. Argyros, S. C. Fleming, and B. T. Kuhlmeiy, "Fiber-drawn double split ring resonators in the terahertz range," *Opt. Mater. Express* **2**, 1254–1259 (2012).
6. J. B. Pendry, "Negative refraction makes a perfect lens," *Phys. Rev. Lett.* **85**, 3966–3969 (2000).
7. Z. Jacob, L. V. Alekseyev, and E. Narimanov, "Optical hyperlens: far-field imaging beyond the diffraction limit," *Opt. Express* **14**, 8247–8256 (2006).
8. M. Yan and N. A. Mortensen, "Hollow-core infrared fiber incorporating metal-wire metamaterial," *Opt. Express* **17**, 14851–14864 (2009).
9. S. Atakaramians, A. Argyros, S. C. Fleming, and B. T. Kuhlmeiy, "Hollow-core waveguides with uniaxial metamaterial cladding: modal equations and guidance conditions," *J. Opt. Soc. Am. B* **29**, 2462–2477 (2012).
10. S. Atakaramians, A. Argyros, S. C. Fleming, and B. T. Kuhlmeiy, "Hollow-core uniaxial metamaterial clad fibers with dispersive metamaterials," *J. Opt. Soc. Am. B* **30**, 851–867 (2013).
11. J. Y. Yan, L. Li, and J. Xiao, "Ring-like solitons in plasmonic fiber waveguides composed of metal-dielectric multilayers," *Opt. Express* **20**, 1945–1952 (2012).

12. A. Argyros, "Microstructures in polymer fibres for optical fibres, THz waveguides, and fibre-based metamaterials," *ISRN Optics* **2013**, 1–22 (2013).
13. R. Melik, E. Unal, N. K. Perkgoz, C. Puttlitz, and H. V. Demir, "Metamaterial-based wireless strain sensors," *Appl. Phys. Lett.* **95**, 011106 (2009).
14. P. P. Banerjee and J. M. Jarem, *Computational Methods for Electromagnetic and Optical Systems* (CRC Press, 2000).
15. E. Popov, ed., *Gratings: Theory and Numeric Applications* (Institut Fresnel, 2012).
16. J. Schesser and G. Eichmann, "Propagation of plane waves in biaxially anisotropic layered media," *J. Opt. Soc. Am.* **62**, 786–791 (1972).
17. J. B. Titchener and J. R. Willis, "The reflection of electromagnetic waves from stratified anisotropic media," *IEEE Trans. Antennas Propag.* **39**, 35–39 (1991).
18. T. M. Grzegorzczuk, X. Chen, J. Pacheco, J. Chen, B. I. Wu, and J. A. Kong, "Reflection coefficients and Goos-Hänchen shifts in anisotropic and bianisotropic left-handed metamaterials," *Prog. Electromagn. Res.* **51**, 83–113 (2005).
19. E. L. Tan, "Recursive asymptotic impedance matrix method for electromagnetic waves in bianisotropic media," *IEEE Microwave Wireless Compon. Lett.* **16**, 351–353 (2006).
20. K. V. Sreekanth and T. Yu, "Long range surface plasmons in a symmetric graphene system with anisotropic dielectrics," *J. Opt.* **15**, 055002 (2013).
21. E. Popov and M. Nevière, "Maxwell equations in Fourier space: fast-converging formulation for diffraction by arbitrary shaped, periodic, anisotropic media," *J. Opt. Soc. Am. A* **18**, 2886–2894 (2001).
22. K. Watanabe, R. Petit, and M. Nevière, "Differential theory of gratings made of anisotropic materials," *J. Opt. Soc. Am. A* **19**, 325–334 (2002).
23. K. Watanabe, J. Pistora, M. Foldyna, K. Postava, and J. Vlcek, "Numerical study on the spectroscopic ellipsometry of lamellar gratings made of lossless dielectric materials," *J. Opt. Soc. Am. A* **22**, 745–751 (2005).
24. T. Magath, "Coupled integral equations for diffraction by profiled, anisotropic, periodic structures," *IEEE Trans. Antennas Propag.* **54**, 681–686 (2006).
25. L. Li, "Use of Fourier series in the analysis of discontinuous periodic structures," *J. Opt. Soc. Am. A* **13**, 1870–1876 (1996).
26. L. Li, "Oblique-coordinate-system-based Chandezon method for modeling one-dimensionally periodic, multilayer, inhomogeneous, anisotropic gratings," *J. Opt. Soc. Am. A* **16**, 2521–2531 (1999).
27. A. Maurel, J.-F. Mercier, and S. Félix, "Wave propagation through penetrable scatterers in a waveguide and through a penetrable grating," *J. Acoust. Soc. Am.* **135**, 165–174 (2014).
28. E. Popov, M. Nevière, B. Gralak, and G. Tayeb, "Staircase approximation validity for arbitrary-shaped gratings," *J. Opt. Soc. Am. A* **19**, 33–42 (2002).
29. P.-H. Tsao, "Derivation and implications of the symmetry property of the permittivity tensor," *Am. J. Phys.* **61**, 823–825 (1993).
30. G. Tayeb, "Contribution à l'étude de la diffraction des ondes électromagnétiques par des réseaux. Réflexions sur les méthodes existantes et sur leur extension aux milieux anisotropes," Ph.D. dissertation, No. 90/Aix 3/0065 (University of Aix-Marseille, 1990).
31. D. R. Smith and D. Schurig, "Electromagnetic wave propagation in media with indefinite permittivity and permeability tensors," *Phys. Rev. Lett.* **90**, 077405 (2003).
32. V. Pagneux, "Multimodal admittance method and singularity behaviour at high frequencies," *J. Comp. App. Maths.* **234**, 1834–1841 (2010).
33. S. Félix, A. Maurel, and J.-F. Mercier, "Local transformation leading to an efficient Fourier modal method for perfectly conducting gratings," *J. Opt. Soc. Am. A* **31**, 2249–2255 (2014).
34. Y. Huang, B. Zhao, and L. Gao, "Goos-Hänchen shift of the reflected wave through an anisotropic metamaterial containing metal/dielectric nanocomposites," *J. Opt. Soc. Am. A* **29**, 1436–1444 (2012).

35. Parametrization of the nut shapes is given (1) with $y_1/b = 0.175 \cos t + 2.5$, $a_1(y_1)/b = 0.15(y_1) + (y_1 - 5)^2/2 + 0.125 \sin t - 0.4$ and (2) with $y_2/b = 0.175 \cos t + 2.5$, $a_2(y_2)/b = 0.3y_2/H + 2(y_2/H - 2.5)^2 + 0.125 \sin t - 0.4$.
36. C. Hazard and E. Lunéville, "An improved multimodal approach for nonuniform acoustic waveguide," *IMA J. Appl. Math.* **73**, 668–690 (2007).
37. A. Maurel, S. Félix, and J.-F. Mercier, "Enhanced transmission through gratings: structural and geometrical effects," *Phys. Rev. B* **88**, 115416 (2013).
38. K. Watanabe, "Numerical integration schemes used on the differential theory for anisotropic gratings," *J. Opt. Soc. Am. A* **19**, 2245–2252 (2002).